PHYSICAL REVIEW E **103**, 052414 (2021)

Remote firing propagation in the neural network of *C. elegans*

Qiwei Shen and Zonghua Liu[*]
School of Physics and Electronic Science, East China Normal University, Shanghai 200062, People's Republic of China

(Received 30 January 2021; revised 4 April 2021; accepted 10 May 2021; published 27 May 2021)

Understanding the mechanisms of firing propagation in brain networks has been a long-standing problem in the fields of nonlinear dynamics and network science. In general, it is believed that a specific firing in a brain network may be gradually propagated from a source node to its neighbors and then to the neighbors' neighbors and so on. Here, we explore firing propagation in the neural network of *Caenorhabditis elegans* and surprisingly find an abnormal phenomenon, i.e., *remote firing propagation* between two distant and indirectly connected nodes with the intermediate nodes being inactivated. This finding is robust to source nodes but depends on the topology of network such as the unidirectional couplings and heterogeneity of network. Further, a brief theoretical analysis is provided to explain its mechanism and a principle for remote firing propagation is figured out. This finding provides insights for us to understand how those cognitive subnetworks emerge in a brain network.

DOI: 10.1103/PhysRevE.103.052414

I. INTRODUCTION

The study of signal propagation has been a long-standing topic in various brain networks, especially the human brain network, where one of the key problems is to understand how brain functions emerge from external stimuli or how different cognitive subnetworks are activated to respond to different external stimuli. For this purpose, intense studies have been made on the synchronization of dynamical systems [1–3]. Recently, much attention has been paid to the aspects of partial synchronization [4], including chimera state, remote synchronization, and cluster synchronization. The chimera state represents the coexistence of coherent and incoherent dynamics [5]. One of its applications is to explain the unihemispheric sleep in aquatic animals and migrating birds [6,7], including the effect of first-night sleep of human beings [8,9]. It is even pointed out that there are cognitive chimera states [10] and multiscale chimera states in human brain networks [11], which may help us to understand the mechanism of the diversity of brain functions. Remote synchronization represents the synchrony among the leaf nodes of a hub but not synchronized with the hub, i.e., the synchronized nodes are not directly connected [12]. It is found that remote synchronization does exist in brain networks and can be extended to distant nodes when two or more star graphs are connected [13]. This finding may help us to understand how different brain functions emerge from their corresponding parts of the brain network. While cluster synchronization represents the case where the oscillators of the network are automatically evolved into different synchronized clusters but the oscillators in different clusters are not synchronized with each other [14,15].

Instead of synchronization, an alternative approach to understand the mechanisms of brain functions is to study how functional cognitive subnetworks emerge from a brain network such as the anatomical brain network. Toward this aim, some efforts have been paid to the aspect of signal amplification in complex networks [16]. It is revealed that weak signals can be amplified by the feature of heterogeneity of scale-free networks [17,18]. Recently, the attention has been focused on how network topologies influence signal or perturbation spreading [19,20]. It is found that both the network topology and the node's dynamics will seriously influence the patterns of propagation. This problem is closely related to the change of brain states during the natural wake-sleep cycle, such as the repeated cycles of nonrapid-eye-movement and rapid-eye-movement sleep, ranging from states of deep unconsciousness to ordinary wakefulness [21].

In sum, these studies are mainly focused on the stabilized states but pay little attention to the evolutionary processes. It is now well known that the functional cognitive activity of the brain is a robust transient process [22–24], which is neither a state of equilibrium nor an exactly periodic oscillation. For a brain to effectively adapt to handle multiple flexible cognitive processes, such as the general sequential dynamics of metastable brain states that are activated by internal or environmental stimuli, it must be able to work in transient modes for a specific cognitive task [25,26]. Therefore, it is more interesting to study the detailed process of signal propagation, especially on some real brain networks.

For this purpose, in this work, we study signal propagation in a neural network by choosing one node as the signal source node and all the other nodes as the target nodes. Considering that signal propagation is in fact the firing propagation in neuron systems, we here study how firing is propagated from an activated source node to all the target nodes. For convenience, we consider a real neural network with small size, i.e., the network of *Caenorhabditis elegans* (*C. elegans*). To make our study closer to reality, except the real neural network substrate, we let the nodes' dynamics be represented by neural models and pay attention to the evolutionary or transient

---

[*] zhliu@phy.ecnu.edu.cn

process. In contrast to the general assumption that a firing will be gradually spread out from a source node to its neighbors and then to the neighbors' neighbors and so on, we surprisingly find an abnormal phenomenon, i.e., remote propagation between distant nodes without the activation of intermediate nodes. This finding is robust to different source nodes and also works for nonlinear negative feedback coupling. Further, we change the unidirectional network of *C. elegans* into a bidirectional network or consider other networks such as the random network, and find that the abnormal phenomenon disappears. A brief theoretical analysis is provided to explain its mechanism and further, a principle for remote firing propagation is figured out. Thus, this finding may help us to understand how a functional brain network emerges from the brain structure network, such as why each specific cognitive subnetwork is distributed in different regions of the brain.

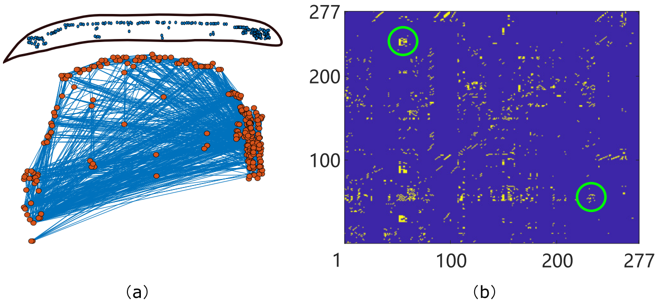

(a) (b)

FIG. 1. The neural network of *C. elegans* from Ref. [33]. (a) shows its physical structure, where the up part represents the locations of all the 277 nodes distributed in *C. elegans* and the low part represents the connections among all the nodes. (b) shows its adjacent matrix where the two blue circles reflect the asymmetry caused by the directional links.

II. A MODEL OF FIRING PROPAGATION IN THE NEURAL NETWORK OF *C. ELEGANS*

For the purpose of understanding the underlying mechanisms of brain functions, some pioneering works have been done so far and it is revealed that synchronization of neuronal ensembles in the network of the cerebral cortex is the base of various neurobiological processes [6,7,27]. However, most of these researches are focused on the topic of partial synchronization, such as the chimera state [5,28,29], remote synchronization [12,13,30], and cluster synchronization [31,32]. On the other hand, the efficiency of brain functions also depends on the firing propagation in the brain network but little attention has been paid to this problem. It is well known that in the performance of a normal brain function, each neuron receives electrical signals via its treelike dendrites, connected via synaptic inputs from other neurons. Thus, the efficiency of firing propagation will seriously influence the neuronal activity that appears to drive the rhythms over different timescales. To obtain some insights on this key problem, we here focus on how firing is propagated on real brain networks, i.e., how the topology of a brain network influences firing propagation. For simplicity, we consider the neural network of *C. elegans* with relatively small size as the first step and hope that the obtained results can be extended to those real networks with larger size, such as the real human brain networks.

Specifically, we take the neural network of *C. elegans* from Ref. [33] as our substrate, which has 277 nodes and 2105 directional links. Figure 1(a) shows its physical structure, where the up part represents the locations of all the 277 nodes distributed in the *C. elegans* and the low part represents the connections among all the nodes. We see that it is a heterogeneous network with distributed nodes degrees. Figure 1(b) shows its adjacent matrix. It is an asymmetric matrix, because its element A_{ij} represents the directional link from the node j to node i. As an example, the two blue circles of Fig. 1(b) show two small symmetric regions along the diagonal line. It is easy to see that they are significantly different, confirming the asymmetry of the adjacent matrix in the real neural network of *C. elegans*.

Based on the adjacent matrix of Fig. 1(b), we now let each node be represented by the Hindmarsh-Rose (HR) model, which was proposed for the neuronal bursting of pond snail Lymnaea by Hindmarsh and Rose in 1984 [34]. The HR model consists of three variables $x(t)$, $y(t)$, and $z(t)$, where x is the membrane potential, y is associated with the fast current Na^+ or K^+, and z with the slow current, for example, Ca^{2+}. Its dynamical equations are as follows:

$$\begin{aligned}\frac{dx_i}{dt} &= y_i + bx_i^2 - ax_i^3 - z_i + I_{\mathrm{ext}} + \lambda\Sigma_{j=1}^{N}A_{ij}(x_j - x_i),\\ \frac{dy_i}{dt} &= c - dx_i^2 - y_i,\\ \frac{dz_i}{dt} &= r[e(x_i - x_0) - z_i],\end{aligned} \tag{1}$$

where i represents the node i with $i \in [1, N]$ and $N = 277$, I_{ext} is the external current input, λ is the coupling strength, and the parameters are taken as $a = 1.0$, $b = 3.0$, $c = 1.0$, $d = 5.0$, $r = 0.006$, $e = 4.0$, and $x_0 = -1.60$ [35]. A_{ij} is the adjacent matrix and can be represented as follows:

$$A_{ij} = \begin{cases} 1, & \text{for a coupling from node } j \text{ to node } i\\ 0, & \text{otherwise.}\end{cases} \tag{2}$$

Equation (1) will return to the case of a single neuron when $\lambda = 0$. In this case, with the increase of I_{ext}, a single neuron will show different periodic behaviors and even chaotic bursts [see Fig. 2(a) for its bifurcation diagram]. From Fig. 2(a) we see that there is a critical $I_{\mathrm{ext}}^c \approx 1.309$. The single neuron will be in the firing status when $I_{\mathrm{ext}} > I_{\mathrm{ext}}^c$ and no firing when $I_{\mathrm{ext}} < I_{\mathrm{ext}}^c$. For $I_{\mathrm{ext}} > I_{\mathrm{ext}}^c$, the system will be period 1 for $1.309 < I_{\mathrm{ext}} < 1.563$, period 2 for $1.563 < I_{\mathrm{ext}} < 2.085, \ldots,$ and chaotic for $2.915 < I_{\mathrm{ext}} < 3.40$. Figures 2(b)–2(e) show four examples for $I_{\mathrm{ext}} = 1.31$ (period 1), 2.0 (period 2), 3.0 (chaotic), and 3.5 (period 1), respectively.

When $\lambda > 0$, Eq. (1) represents coupled dynamics through the network of *C. elegans*. In this case, the brain system is organized into processing streams, along which the firings induced by the external input I_{ext} will be propagated to other parts of the network and thus activates a specific brain function. Our purpose here is to study how the firing is propagated in this neural network of *C. elegans* and how activating clusters of nodes are formed. For this purpose, our idea is to let I_{ext} be a value slightly smaller than the critical point I_{ext}^c so

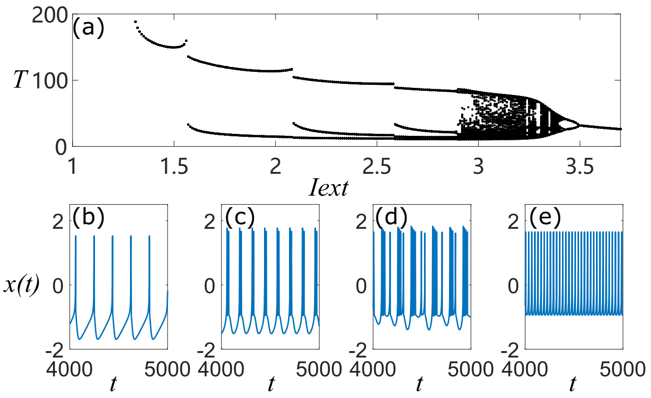

FIG. 2. Dynamical behaviors of a single neuron of the HR model where (a) represents the bifurcation diagram and (b)–(e) represent four typical dynamics for $I_{\text{ext}} = 1.31$ (period 1), 2.0 (period 2), 3.0 (chaotic), and 3.5 (period 1), respectively.

that the whole brain network is inactivated when there are no initial activated nodes. That is, we fix $I_{\text{ext}} = 1.3$ in this work. In this sense, the inactive oscillators in the network of *C. elegans* are similar to an inactive environment used in environmental coupling [36]. Then, we will add another external stimulus to a specific node as the input signal and call this node the source node. In general, we let the input stimulus satisfy the condition that the source node should be activated. We will pay attention to how the firing of the source node is propagated to other nodes of the network and then try to figure out the underlying mechanisms for the emergence of brain functions.

III. NUMERICAL SIMULATIONS ON DIFFERENT SOURCE NODES

In numerical simulations, we consider only one node as the source node s while all the other nodes as target nodes. We consider the external input I_{ext} of Eq. (1) as a common background for all the nodes, including both the source and target nodes, and let I_s be an additional external stimulus only for the source node s. For convenience, we call I_{ext} the background stimulus while I_s is called the external stimulus. Thus, for the source node s, the first equation of Eqs. (1) will become

$$\frac{dx_s}{dt} = y_s + bx_s^2 - ax_s^3 - z_s + I_{\text{ext}} + I_s + \lambda \Sigma_{j=1}^{N} A_{sj}(x_j - x_s). \tag{3}$$

While for all the target nodes, Eqs. (1) will remain unchanged. To detect the firing propagation, we set a firing threshold as $x_c = 0$. A target node i will be considered as firing propagated or activated once its x variable reaches $x_i \geqslant x_c$, i.e., no matter whether it is a burst or spike [see Figs. 2(b)–2(e) for different firing behaviors]. Further, we let I_s be large enough so that it can produce a firing at the source node when $\lambda = 0$. By this way, we can measure whether the firing of the source node s is propagated to target nodes or not.

We first consider the case of taking the external stimulus $I_s = 1.7$ and the coupling strength $\lambda = 0.25$. Very interestingly, we find that the firing can be either propagated or not, depending on the chosen source nodes. Figure 3(a) shows the case of successfully propagated firing from the source node s to one of its nearest neighboring nodes, where the red and blue lines represent the time evolutions of x variables at the source node 15 and the target node 47, respectively. The inset shows the local structure of the source node 15. We see that the source node 15 has 12 neighboring nodes with 1 in-coming link and 12 outgoing links, where the neighboring node 49 is a bidirectional link. As the target node 47 receives a coupling from the source node 15, it is also activated. Figure 3(b) shows the case where the firing cannot be propagated and even cannot be successfully generated at the source node (see the red and blue lines for the time evolutions of x variable at the source node 73 and one of its neighboring nodes 5, respectively). The inset shows the local structure of the source node 73, which has 10 neighboring nodes with 4 incoming links and 6 outgoing links. We see that both the red and blue lines do not reach the firing threshold $x_c = 0$. Why is it that source node 73 cannot be activated by the same external stimulus $I_s = 1.7$ as that in Fig. 3(a)? Their graphs of insets may tell us the answer. We see that source node 73 has multiple incoming links, in contrast to Fig. 3(a) with only one incoming link. We will discuss it further in Fig. 4 and also provide a theoretical explanation in Sec. VI. For obtaining a global picture of firing propagation, we successively choose every node as the source node for one time and count how many target nodes can be activated to reach $x_i \geqslant x_c$. We let n_s be the number of activated nodes in the whole network by the source node s, including both the activated source node and the activated target nodes. Figure 3(c) shows the dependence of n_s on the chosen source

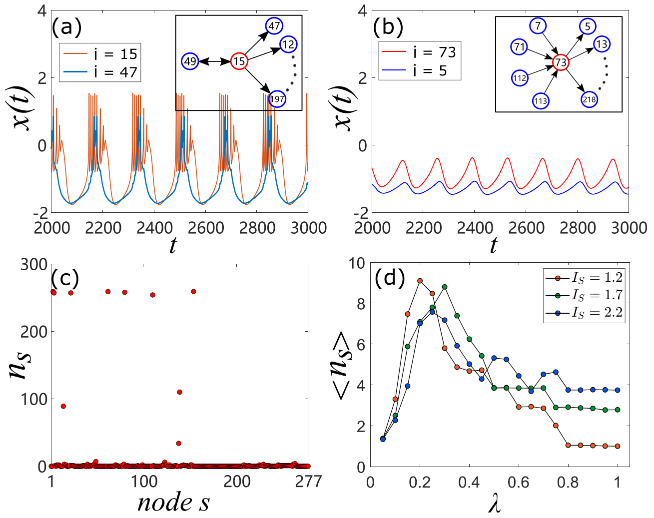

FIG. 3. Firing propagation in the neural network of *C. elegans*, with $I_s = 1.7$ and $\lambda = 0.25$ in (a)–(c). (a) and (b) represent the cases of successfully and unsuccessfully propagated firings from the source nodes to their nearest neighbors, respectively, where the insets show the local structures of the source nodes and the red and blue lines represent the time evolutions of x variables at the source nodes and their neighboring nodes, respectively. (c) shows the dependence of the number of activated nodes n_s on the source node s. (d) shows the dependence of $\langle n_s \rangle$ on the coupling strength λ where the three curves represent the cases of taking the external stimulus as $I_s = 1.2,\ 1.7$, and 2.2, respectively.

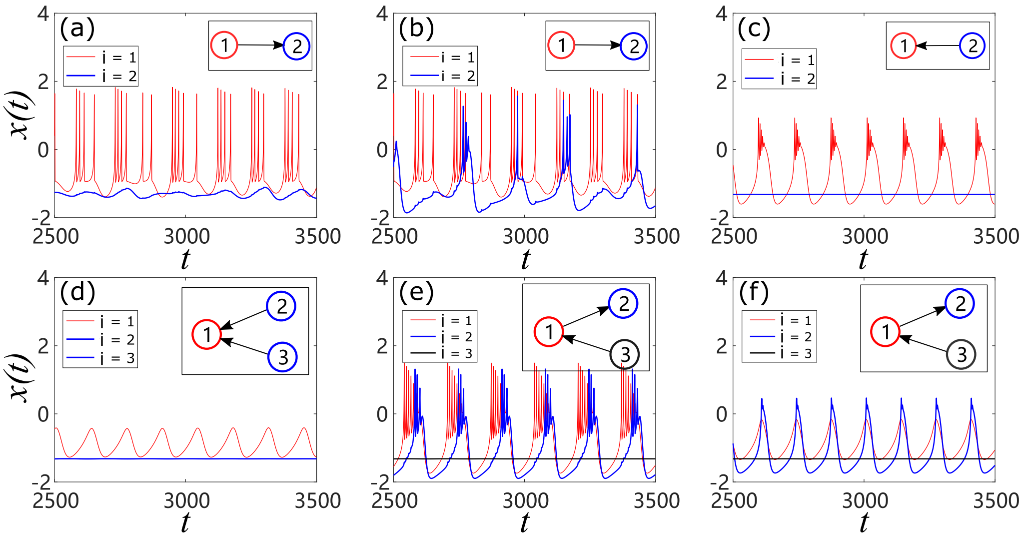

FIG. 4. Firing propagation in typical motifs with $I_s = 1.7$ where the red line represents the dynamics of the source node s and the blue and black lines represent the dynamics of the target nodes. (a) and (b) represent the case of only one target node with coupling from the source node s to the target node, with $\lambda = 0.05$ in (a) and $\lambda = 0.2$ in (b). (c) and (d) represent the case of coupling from the target nodes to the source node s, where the coupling strength is fixed as $\lambda = 0.5$ and there is one target node in (c) but two target nodes in (d). (e) and (f) represent the case of two target nodes with one coupling from the source node s to the target node and another one opposite, with $\lambda = 0.25$ in (e) and $\lambda = 0.95$ in (f).

node s. We see that n_s is significantly different from one to another and can be divided into three classes: (1) n_s is close to N, implying that the firing is globally propagated. (2) $n_s = 0$, indicating that the firing cannot be even successfully generated at the source node s. (3) n_s is in between the first two cases, i.e., firing is propagated to part of the network. We will pay more attention to class (3).

Let $\langle n_s \rangle$ be the average of n_s on all the source nodes s for fixed I_s and λ. We find that $\langle n_s \rangle$ depends on both the parameters I_s and λ. Figure 3(d) shows the dependence of $\langle n_s \rangle$ on the coupling strength λ where the three curves represent the cases of taking the external stimulus as $I_s = 1.2,\ 1.7,$ and 2.2, respectively. We see that all three curves are bell shaped, indicating that there is an optimal λ for each fixed I_s.

In sum, three observations can be made from Fig. 3: (i) From (a) we see that the amplitude of the propagated node is smaller than that of the source node s, indicating the decaying of firing. (ii) From (b) we see that the amplitude is not zero but a small value at both the source and propagated nodes, although the source node s is not activated. (iii) From (d) we see that there is an optimal coupling strength λ, in contrast to the general assumption that a larger coupling always favors firing propagation. To understand these observations of Fig. 3, we design a few typical motifs consisting of the source node s and its nearest neighboring nodes only (see the insets of Fig. 4 with $I_s = 1.7$). Figures 4(a) and 4(b) represent the case of only one target node with coupling from the source node s to the target node, with $\lambda = 0.05$ in (a) and $\lambda = 0.2$ in (b). We see that the target node is activated for the larger coupling of $\lambda = 0.2$ in (b) but not for the smaller coupling of $\lambda = 0.05$ in (a), indicating that a larger coupling favors firing propagation rather than that of a smaller coupling. Figures 4(c) and (d) represent the case of coupling from the target nodes to the source node s, where the coupling strength is fixed as $\lambda = 0.5$ and there is one target node in (c) but two target nodes in (d). We see that the source node s can be activated in Fig. 4(c) with reduced amplitude, but cannot be activated in (d), indicating that the incoming coupling from a target node behaves like an obstructor and more such couplings will have stronger power to reduce the firing of the source node. Figures 4(e) and 4(f) represent the case of two target nodes with one coupling from the source node s to the target node and another one opposite, with $\lambda = 0.25$ in (e) and $\lambda = 0.95$ in (f). We see that both source node 1 and target node 2 are influenced by the coupling and stronger coupling will influence more. Comparing the case of Figs. 4(e) and 4(f) with that of Figs. 4(a) and 4(b), we see that their couplings have opposite effects on the target node 2, i.e., enhanced firing in Figs. 4(a) and 4(b) but weakened firing in Figs. 4(e) and 4(f).

Very interestingly, we notice from Fig. 4(f) that the source node 1 has $x_1 < x_c$ and the target node 2 has $x_2 > x_c$, indicating that source node 1 is not activated but the target node 2 is activated. This is an abnormal phenomenon and tells us that both the firing of the source node and its firing propagation come from the competition between its enhancing coupling and weakening coupling. This finding also brings us a new topic: Can a firing be propagated from a source node to a distant target node without the activation of their intermediate nodes? This is an important question in a human brain network as each of its cognitive subnetworks is composed of not only those nodes located in the same local area but also other nodes distributed in different local areas [10]. Here, an open question is how these distributed nodes emerge as a cognitive subnetwork to execute specific brain function or even how the brain functional network emerges from the physical structure network. To go a substantial step toward this open question, we need to recheck the detailed propagation process

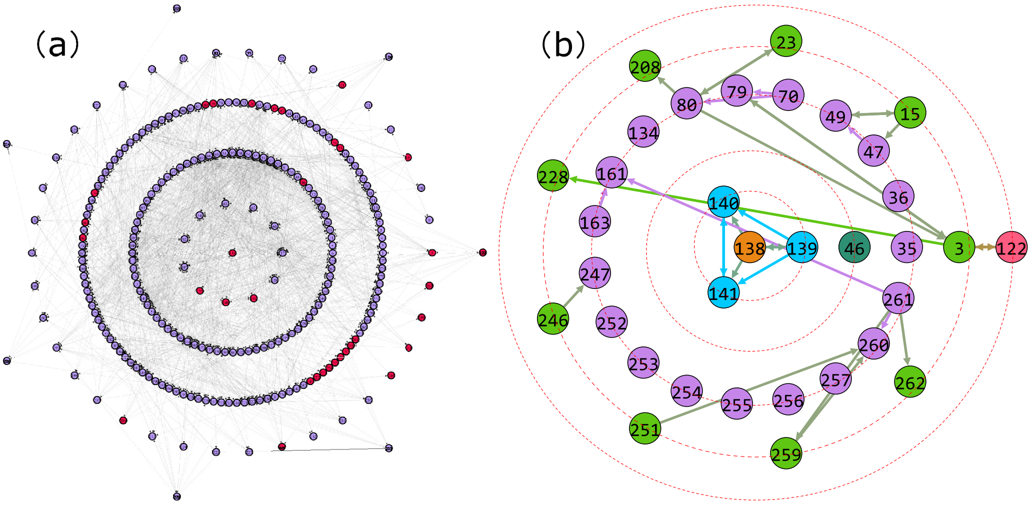

FIG. 5. A typical example of RFP where the source node is chosen as node138 and parameters are taken as $I_s = 1.7$ and $\lambda = 0.25$. (a) The paths of firing propagation in the neural network of *C. elegans* where the central red node is source node 138, other red nodes are the propagated nodes, and the different circles from the center represent the nearest neighboring nodes, the neighbors' neighbors, and so on. (b) A part of the network of (a) with only the firing nodes and the links among them, where the colors of nodes are changed to be different from circle to circle, as a guide for the eyes.

of Fig. 3(c), especially the class (3), and extend the analysis of the motifs of Fig. 4 to the much more complicated case of the neural network of *C. elegans*.

From Fig. 3(c) we notice that some source nodes can be activated and thus their firings will be propagated, while others cannot. For the former, the propagated ranges are different for different source nodes, i.e., some can go to global level with $n_s \approx 260$ while others only go to a small part of nodes with $n_s < 10$. This raises an important question: What is the rule for a firing to be propagated and how does the structure of a brain network influence the propagation range n_s? In general, we may think that firing will be first propagated from the source node to its neighbors and then to neighbors' neighbors and so on. However, after checking all the detailed propagation processes of Fig. 3(c), we surprisingly find that it is not always like that. Sometimes, the nearest neighbors may not be propagated but the neighbors' neighbors or even further non-neighboring nodes can be propagated. This is in sharp contrast to our common sense. We here call it *remote firing propagation* (RFP), i.e., the firing propagation between two distant and indirectly connected nodes with the intermediate nodes being inactivated.

To show RFP in detail, Fig. 5(a) shows such an example of the source node 138 where the network topology is plotted as the center for the source node, the first circle for the nearest neighboring nodes of the source node, and the second circle for the nearest neighbors' neighbors and so on. The red nodes represent all the activated nodes from the source node. As Fig. 5(a) contains all nodes, the connections among them are too dense and thus difficult for us to study the relationship among the activated nodes. To figure out the features of RFP, we simplify Fig. 5(a) into Fig. 5(b) by keeping only the red nodes and those links among them, i.e., remove all the other nodes and their links, which will not influence our analysis. Further, we let the colors of the nodes of Fig. 5(b) be different from circle to circle so that their connections can be easily distinguished. From Fig. 5(b) we see that only the three nodes 139–141 of the first circle are connected to source node 138 and thus form a core cluster of four connected nodes, while all the other nodes are not directly connected to them, indicating that they must be indirectly connected to the core cluster. Moreover, some of them even have no connections to others such as the nodes 46, 35, and 253, etc., implying that they are isolated to all the other activated nodes. This finding may open a new window for us to understand the underlying mechanisms for the emergence of cognitive subnetworks and brain functional networks. We will explain it theoretically in Sec. VI.

IV. FIRING PROPAGATION IN OTHER NETWORKS

It is important to check whether the phenomenon of RFP is only observed in brain networks or can be also observed in other complex networks. For this purpose, we consider two specific networks, both with the same number of nodes and the same number of total links as that of the neural network of *C. elegans*.

The first one is the bidirectional neural network of *C. elegans* where all the directional couplings are changed into bidirectional couplings and other parameters are kept unchanged [see the insets of Figs. 6(a) and 6(b)]. By doing the same steps as in Sec. III, we find that RFP does not show up anymore. Moreover, the firing propagation process is significantly different from the case of directional couplings. Figure 6 shows the results corresponding to Fig. 3 where Figs. 6(a)– 6(d) correspond to (a)–(d) of Fig. 3, respectively. Comparing Fig. 6(a) with Fig. 3(a), we see that the firings are bursts in Fig. 3(a) but spikes in Fig. 6(a). Comparing Fig. 6(b) with Fig. 3(b), we see that their difference is even significantly large, i.e., there are no firings in Fig. 3(b) but firings in Fig. 6(b). A consequence of these differences is that there is a class (3) in Fig. 3(c) but no class (3) in Fig. 6(c). A further consequence is that the average number of activated nodes is $\langle n_s \rangle < 10$ in Fig. 3(d) but can reach almost all of

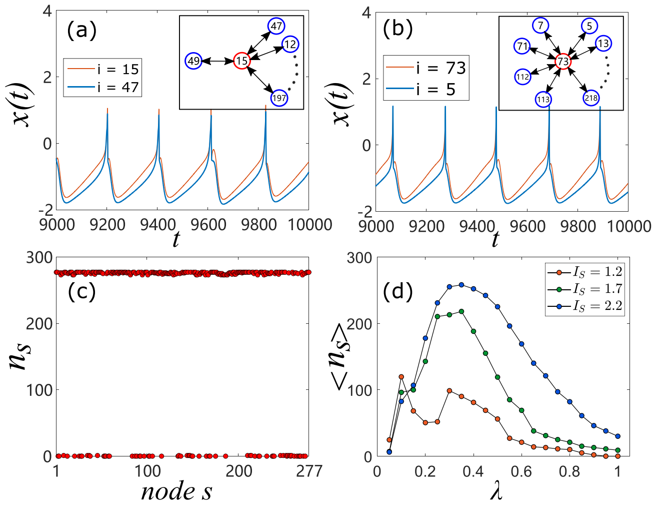

FIG. 6. Firing propagation in the bidirectional neural network of *C. elegans* where the parameters are kept the same as in Fig. 3, except the directional couplings are changed into bidirectional couplings. (a)–(d) correspond to (a)–(d) of Fig. 3, respectively.

the nodes in Fig. 6(d), i.e., the maximum $\langle n_s \rangle \approx 258$. The underlying mechanism is that the bidirectional couplings make the outgoing couplings be approximately doubled and thus make the firing of the source node be quickly propagated to its neighbors and neighbors' neighbors and so on. In this sense, there are no longer purely obstructors and thus the competition between the enhancing coupling and weakening coupling is broken, resulting in no space for RFP.

The second one is a directional random network from the directional neural network of *C. elegans* and is constructed as follows. We keep all 277 nodes and 2105 directional links of the neural network of *C. elegans* from Ref. [33] but let the 2105 directional links be randomly rearranged among the 277 nodes. For example, we randomly choose two nodes i and j and let them have a directional link from node i to node j. We will abandon it if this directional link already exists. Then, we reduce one from the 2105 directional links. We continue this process until all 2105 directional links have gone. In this way, different directional random networks can be obtained. Based on the obtained directional random networks, our numerical simulations show that there is no RFP in any one of them. Take one of these directional random networks as an example. Figure 7 shows the results corresponding to Fig. 3 where (a)–(d) correspond to (a)–(d) of Fig. 3, respectively. Comparing the inset of Fig. 7(a) with that of Fig. 3(a), we see that the number of source node's neighboring nodes changes from 12 (1 incoming link and 12 outgoing links, with one being a bidirectional link) in Fig. 3(a) to 16 (10 incoming links and 6 outgoing links) in Fig. 7(a). This change of network topology causes the change of dynamics from Fig. 3(a) with activation to Fig. 7(a) with inactivation. That is, because of too many incoming links in Fig. 7(a), its source node 15 becomes inactivated. Similarly, comparing the inset of Fig. 7(b) with that of Fig. 3(b), we see that the number of the source node's neighboring nodes changes from 10 (4 incoming links and 6 outgoing links) in Fig. 3(b) to 14 (6 incoming links and 8 outgoing links) in Fig. 7(b). Very interestingly, this change

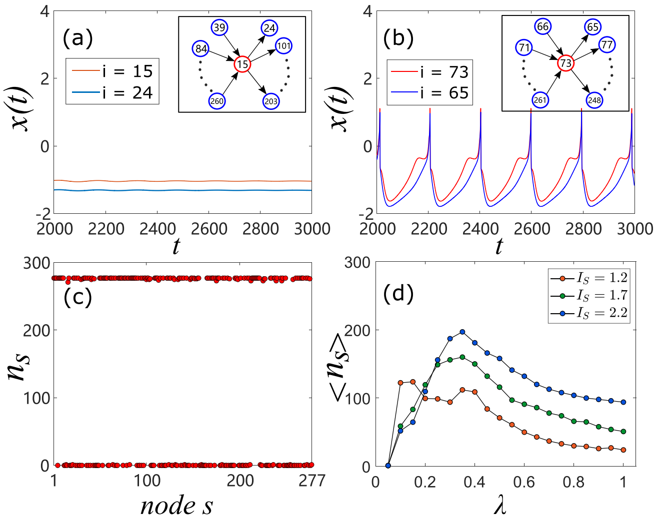

FIG. 7. Firing propagation in the directional random network from the neural network of *C. elegans* where the parameters are kept the same as in Fig. 3, except the directional couplings are randomly rearranged among the 277 nodes with overlapped links avoided. (a)–(d) correspond to (a)–(d) of Fig. 3, respectively.

of network topology causes an inverse change of dynamics, i.e., from Fig. 3(b) with inactivation to Fig. 7(b) with activation. However, a new point here is that both Fig. 3(b) and Fig. 7(b) have a number of incoming links, thus the activation of Fig. 7(b) implies that other features of a network such as the community also take effect in firing propagation. Comparing Figs. 7(c) and 7(d) with Figs. 6(c) and 6(d), respectively, we see that they are similar to each other, indicating that they have a similar underlying mechanism to break the competition between the enhancing coupling and weakening coupling and thus result in no space for RFP.

In sum, we notice a common feature from the relationship between $\langle n_s \rangle$ and λ in Figs. 3(d), 6(d), and 7(d) that $\langle n_s \rangle$ is switched at some medium coupling strength, e.g., more nodes are activated for the case of $I_s = 1.2$ when $\lambda = 0.1$, but more nodes are activated for the case of $I_s = 2.2$ when $\lambda = 0.8$. Then, an interesting question is what is the underlying mechanism for this switching phenomenon? To figure out the answer, we go back to Fig. 2. From Fig. 2(a) we see that the firing period T depends sensitively on the bifurcation parameter I_{ext}. And from Figs. 2(b)–2(e) we see that the firing behaviors are closely related to I_{ext}, i.e., the firing period T. In this sense, a shorter firing period T of source node will have a higher frequency to activate its neighbors than that of a longer firing period T of source node. When the coupling strength λ is small in Eq. (1), such as $\lambda < 0.1$, this effect will increase with λ and result in a faster increase of $\langle n_s \rangle$ for the shorter firing period T of the source node than that for the longer firing period T of the source node, confirming the observed results for $\lambda = 0.1$. However, when the coupling strength λ is large in Eq. (1), such as $\lambda > 0.3$, a nearest neighbor of the source node will get a larger resistance from its neighbors, i.e., the second nearest neighbors of the source node. When this resistance is greater than the influence from the source node, the increase of λ will prevent the further firing propagation from the nearest neighbors of the source node and result in a slower increase of $\langle n_s \rangle$ for the shorter firing period T of source node than that for the longer firing period T of source node, confirming the observed results for $\lambda = 0.8$. This may be the mechanism for the observed switching phenomenon.

V. FIRING PROPAGATION BY NONLINEAR NEGATIVE FEEDBACK COUPLING

The negative feedback coupling of Eq. (1) is usually regarded as a diffusive coupling and represents the electric coupling, provided that it is bidirectional. In this case, Chen *et al.* found that stimulating a single node, i.e., the largest-degree node, may induce the firing of the whole network [37]. However, this is not the coupling considered in this work, as the asymmetric matrix A_{ij} of Eq. (1) symbolizes the directions of couplings, i.e., the coupling of Eq. (1) is not bidirectional. In this sense, the directional coupling of Eq. (1) is more like a chemical coupling, i.e., having the directionality of chemical coupling.

It is well known that there are both electric and chemical couplings in neural systems. To reflect this fact, it is necessary to consider both couplings at the same time [38–41]. For example, Pournaki *et al.* considered both electric and chemical couplings in the neuronal networks of *C. elegans* and found that chimeralike states can be hard to identify in real-world networks [38]. Following Ref. [38], a key variable of chemical coupling is the nonlinear sigmoidal function

$$S(x) = \frac{1}{1 + \exp\left[-\lambda_{\mathrm{syn}}(x - \theta_{\mathrm{syn}})\right]}, \tag{4}$$

where the parameters are usually taken as $\theta_{\mathrm{syn}} = -0.25$ and $\lambda_{\mathrm{syn}} = 10$. By this sigmoidal function, the chemical coupling can be described as

$$\text{chemical coupling} = -g_{\mathrm{ch}}(x_i - V_{\mathrm{syn}})\Sigma_{j=1}^{N} A_{ij} S(x_j), \tag{5}$$

where g_{ch} is the coupling strength and $V_{\mathrm{syn}} = 2$ is the reversal potential of the synaptic current.

Motivated by Eq. (5), we would like to replace the linear coupling $\lambda \Sigma_{j=1}^{N} A_{ij}(x_j - x_i)$ of Eq. (1) by a nonlinear coupling $-\lambda(x_i - V_{\mathrm{syn}})\Sigma_{j=1}^{N} A_{ij}[S(x_j) - S(x_i)]$. In this way, Eq. (1) will become

$$\begin{aligned}
\frac{dx_i}{dt} &= y_i + bx_i^2 - ax_i^3 - z_i + I_{\mathrm{ext}} \\
&\quad - \lambda(x_i - V_{\mathrm{syn}})\Sigma_{j=1}^{N} A_{ij}[S(x_j) - S(x_i)], \\
\frac{dy_i}{dt} &= c - dx_i^2 - y_i, \\
\frac{dz_i}{dt} &= r[e(x_i - x_0) - z_i].
\end{aligned} \tag{6}$$

That is, the linear coupling of Eq. (1) is replaced by the nonlinear coupling of Eq. (6). Correspondingly, Eq. (3) will be replaced by

$$\begin{aligned}
\frac{dx_s}{dt} &= y_s + bx_s^2 - ax_s^3 - z_s + I_{\mathrm{ext}} + I_s \\
&\quad - \lambda(x_s - V_{\mathrm{syn}})\Sigma_{j=1}^{N} A_{sj}[S(x_j) - S(x_s)].
\end{aligned} \tag{7}$$

This nonlinear negative feedback coupling may be considered as a combination of electric and chemical couplings, but its biological aspect remains to be confirmed. Thus, we here consider Eqs. (6) and (7) as an abstract or toy model and only use it to check the robustness of RFP.

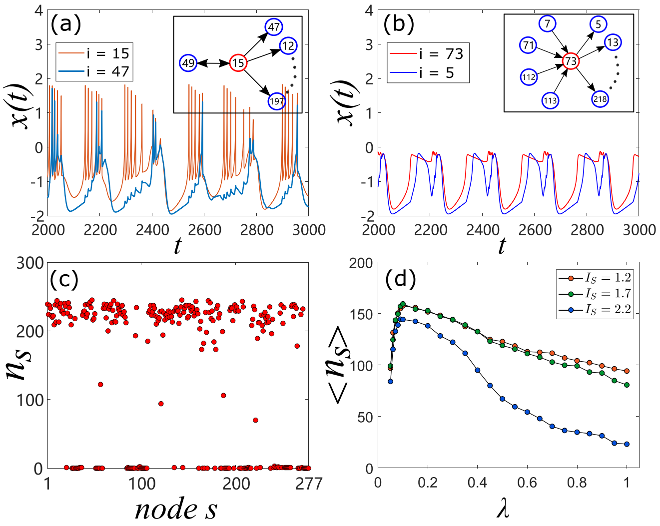

FIG. 8. Case of nonlinear negative feedback coupling for the firing propagation in the neural network of *C. elegans*, with $I_s = 1.7$ and $\lambda = 0.25$ in (a)–(c). All the panels (a)–(d) correspond to that of Figs. 3(a)–3(d), respectively, where the parameters are kept the same.

Doing the same procedures as in Fig. 3, Fig. 8 shows the results by Eqs. (6) and (7). Comparing the corresponding panels between Fig. 3 and Fig. 8, we see that Figs. 8(a) and 8(b) are similar to Figs. 3(a) and 3(b), respectively, but their panels (c) and (d) are of some difference. For their panels (c), there is much more global propagation $\langle n_s \rangle$ in Fig. 8(c) than that in Fig. 3(c), indicating that the nonlinear coupling of Eqs. (6) and (7) favors the firing propagation, while for their panels (d), the switching phenomenon of Fig. 3(d) disappears in Fig. 8(d).

Similarly, Figs. 9(a)–9(d) show the results corresponding to Figs. 4(a)–4(d), respectively. Comparing their corresponding panels, we see that they are qualitatively similar to each other, respectively, implying that the nonlinear coupling of Eqs. (6) and (7) does not change the firing propagation substantially.

Very interestingly, we find that RFP can be also observed in the case of nonlinear negative feedback coupling. Figure 10 shows such an example, corresponding to Fig. 5. From Fig. 10(b) we see that there are no activated nodes in the first circle but there are12 activated nodes in the second circle, confirming the existence of RFP. Therefore, RFP is of robustness in the neural network of *C. elegans*.

VI. A BRIEF THEORETICAL ANALYSIS

In this section, we aim to give a brief theoretical explanation to the observed RFP in Fig. 5. For a single HR neuron, we know from Fig. 2 that it will be activated once its external input I_{ext} is greater than the threshold I_{ext}^c. This rule will still work for a node in the network, i.e., a node will be activated once its total external input is greater than the threshold I_{ext}^c. From Eq. (1) we know that the total external input of

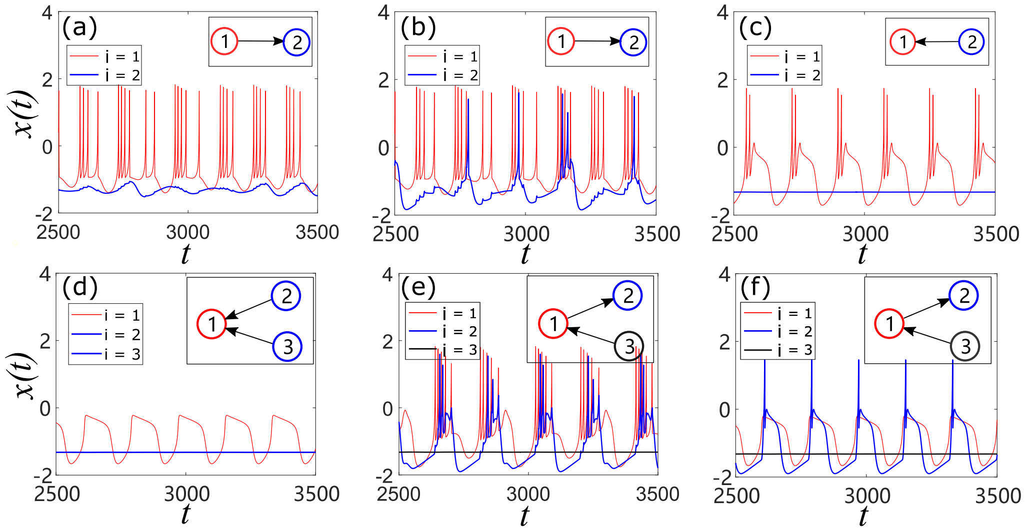

FIG. 9. Case of nonlinear negative feedback coupling for the firing propagation in typical motifs with $I_s = 1.7$ where the red line represents the dynamics of the source node and the blue and black lines represent the dynamics of the target nodes. All the panels (a)–(f) correspond to that of Figs. 4(a)–4(f), respectively, where the parameters are kept the same.

node i is $I_{\text{ext}} + \lambda \Sigma_{j=1}^{N} A_{ij}(x_j - x_i)$, which gives the activating condition

$$I_{\text{ext}} + \lambda \Sigma_{j=1}^{N} A_{ij}(x_j - x_i) > I_{\text{ext}}^{c}. \tag{8}$$

By Eq. (8) we know that the coupling term $\lambda \Sigma_{j=1}^{N} A_{ij}(x_j - x_i)$ is very important for the activation of node i. Node i will be activated when $\lambda \Sigma_{j=1}^{N} A_{ij}(x_j - x_i)$ is positive and larger than $I_{\text{ext}}^{c} - I_{\text{ext}}$. In general, the neighbors of node i can be divided into two classes. One class has positive contribution to the activation of node i, while another class has negative contribution. The nodes in the positive class usually have shorter distance to the source node s than that in the negative class. Therefore, the total coupling $\lambda \Sigma_{j=1}^{N} A_{ij}(x_j - x_i)$ of node i will be a competition or balance between the positive and negative coupling parts. The positive coupling can be considered as a stimulator while the negative as an obstructor. In this sense, a greater number of positive coupling links is better for the activation of node i, while a greater number of negative coupling links will prevent the activation of node i.

While for the source node s, condition (8) will become

$$I_{\text{ext}} + I_s + \lambda \Sigma_{j=1}^{N} A_{sj}(x_j - x_s) > I_{\text{ext}}^{c}. \tag{9}$$

In this case, all the coupling links take negative contribution and thus all of them behave as obstructors. Therefore, a greater number of coupling links will prevent the activation of the source node s more. That is, the source node s will not be

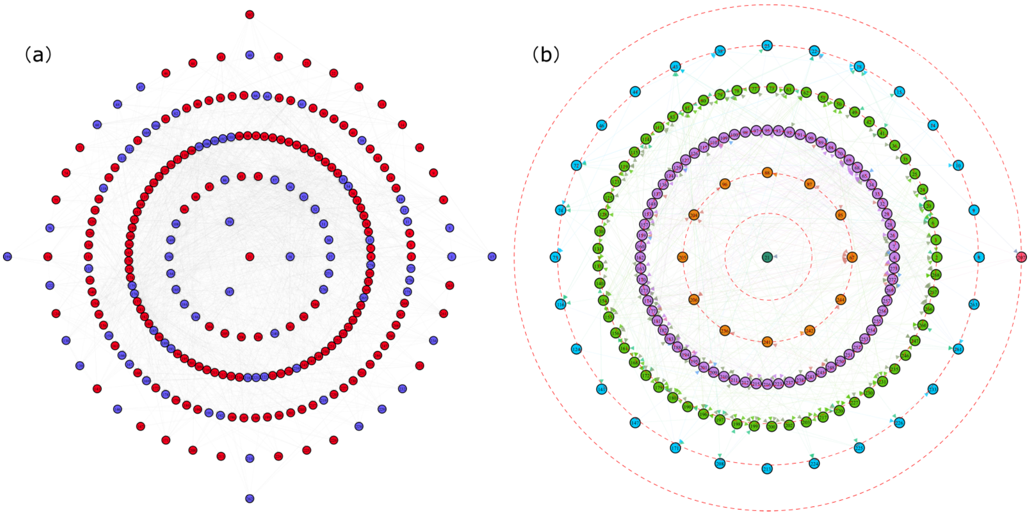

FIG. 10. A typical example of RFP for the case of nonlinear negative feedback coupling of Eqs. (6) and (7) where the source node is chosen as node 21 and parameters are taken as $I_s = 1.7$ and $\lambda = 0.09$. (a) The paths of firing propagation in the neural network of *C. elegans* where the central red node is source node 21, other red nodes are the propagated nodes, and the different circles from the center represent the nearest neighboring nodes, the neighbors' neighbors, and so on. (b) A part of the network of (a) with only the firing nodes and the links among them, where the colors of nodes are changed to be different from circle to circle, as a guide for the eyes.

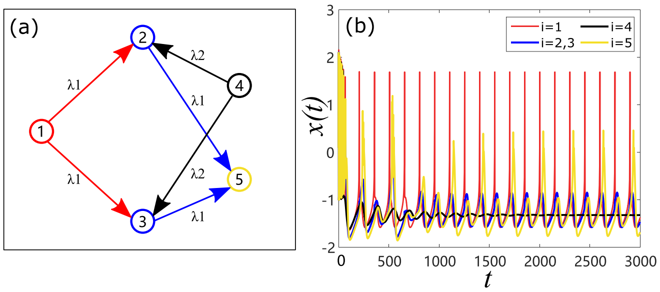

FIG. 11. The mechanism of RFP with $I_s = 0.2$. (a) The schematic figure of RFP where node 1 represents the source node, nodes 2–5 represent the four target nodes, and the arrows denote the directions of couplings. The coupling strength from node 4 is λ_2 and that from other nodes is λ_1. (b) represents the dynamics of all five nodes in (a), with $\lambda_1 = 0.25$ and $\lambda_2 = 0.15$, where the "red," "blue," "black," and "yellow" lines represent node 1, nodes 2 and 3, node 4, and node 5, respectively.

activated once $I_{\text{ext}} + I_s - I^c_{\text{ext}} < -\lambda\Sigma_{j=1}^N A_{sj}(x_j - x_s)$. In this sense, both the coupling strength λ and degree $\Sigma_{j=1}^N A_{sj}$ take important roles for firing propagation, as in the case of echo behavior [42].

According to these analyses, we go back to Fig. 4 and find that all the motifs completely agree with the above analysis. For example, in Fig. 4(a), Eq. (8) is not satisfied as the coupling strength λ is too small. Whereas in Fig. 4(b), Eq. (8) is satisfied as the coupling strength λ is now large enough. In Fig. 4(c), we have only one obstructor, thus Eq. (9) is satisfied. Whereas in Fig. 4(d), the number of obstructors is increased to two, which breaks the condition of Eq. (9). In Fig. 4(e), the coupling strength λ is larger than that of Fig. 4(b) but less than that of Fig. 4(c), implying that the coupling strength is not enough for the obstructor node 3 to prevent the activation of source node 1 but large enough for target node 2 to be activated, i.e., both Eq. (8) and Eq. (9) are satisfied. A similar analysis can be applied to Fig. 4(f).

Based on these analyses, it is now the time for us to explain the mechanism of RFP. For this purpose, we here design a schematic figure to illustrate the principle of RFP [see Fig. 11(a)]. In this schematic figure, we have an activated source node 1 and four target nodes 2–5, where the arrows denote the directions of couplings. We require that the middle nodes 2 and 3 will not be activated but the remote node 5 will be activated. For this purpose, we let node 4 be an obstructor and also let its coupling strength λ_2 be a little different from the coupling strength λ_1 of other nodes. This may be reasonable as node 4 represents the comprehensive effect from other nodes of the network and thus its effective coupling strength cannot be exactly the same as that of other links. Our numerical simulations show that the schematic figure of Fig. 11(a) does generate RFP. Figure 11(b) shows one of such realizations of RFP by choosing $I_s = 0.2$, $\lambda_1 = 0.25$, and $\lambda_2 = 0.15$, and keep other parameters the same as in Fig. 3. Based on this schematic figure, we now conclude the principle of RFP as follows: (i) The system of RFP consists of three parts, i.e., a source node s, a remote node j, and some intermediate nodes k. The source node s should be in the activated status. (ii) The intermediate node k has to receive both the incoming and outgoing couplings and one of its in-coming couplings has to come from the obstructor node. The balance of these couplings should prevent the firing of the intermediate node k but sustain it as an oscillatory behavior of a small amplitude, i.e., $x_k < x_c$. And (iii) the remote node j should only receive couplings from those intermediate nodes with small amplitude oscillations and the sum of these couplings is large enough for the remote node j to be activated.

VII. DISCUSSIONS AND CONCLUSIONS

We have to point out that RFP is fundamentally different from the concept of remote synchronization although they both concern the relationship between indirectly connected nodes. Remote synchronization is currently a hot topic in the fields of nonlinear science and complex networks and represents the synchronization between indirectly connected or distant nodes where the intermediate nodes are not synchronized with them [12,13]. Take the star graph as an example. When the frequency of the central node is largely different from that of leaf nodes, a remote synchronization among all the leaf nodes may appear but the leaf nodes do not synchronize with the central node. While RFP does not pay attention to the synchronization of unconnected nodes but to their firing propagation, i.e., the synchronization among the remote propagated nodes is not necessary. Specifically, we may have only one remote propagated node in RFP, where synchronization cannot be discussed. On the other hand, when we have several remote propagated nodes in RFP and they all have the same distance to the source node, these remote propagated nodes may fire at the same time and thus can be also considered as remote synchronization.

On the other hand, the finding of RFP may provide a new clue to understand the emergence of cognitive subnetworks. It is well known that the structural brain network consists of a huge number of neurons and is thus very complicated. For a specific brain function, the involved neurons are only part of the total neurons but not all of them. It is revealed that these involved neurons form a specific cognitive subnetwork but are distributed in different regions of the brain [10,25,26]. A similar case goes to the resting-state network where its number of links is much less than that at wake and its nodes are also distributed in different regions of the brain [21,43]. Previously, these functional networks are approved by experiments but its microcosmic mechanism remains unclear. Here, RFP shows a possible way for distant nodes to transmit the same firing signal. For class (3) in Fig. 3(c), we observe that different source nodes will have different sets of activated nodes. If we explain each specific set of activated nodes as a subnetwork and the initially activated source node as a task, this cluster of activated nodes will be equivalent to a cognitive subnetwork. Therefore, we may assume that the way of generating RFP is closely related to the way of generating cognitive subnetworks.

In conclusion, we have studied the firing propagation in the directional neural network of *C. elegans* by the HR model and found that the propagated range depends sensitively on the chosen source node, i.e., it can be either global or zero. Specifically, we find a novel phenomenon of RFP and confirm that it cannot be observed in both the bidirectional network of *C. elegans* and the random network. By studying the local patterns of RFP we find the conditions for the appearance of RFP. Based on a brief theoretical analysis, we figure out the principle of RFP. This finding may show insights for us to understand how those cognitive subnetworks emerge among distant nodes of the brain network. Finally, we expect that our schematic figure of RFP provides a framework for experimental scientists to confirm this novel phenomenon of RFP.

ACKNOWLEDGMENTS

This work was partially supported by the National Natural Science Foundation of China under Grants No. 11835003 and No. 82161148012.

[1] A. Pikovsky, M. Rosenblum, and J. Kurths, *Synchronization: A Universal Concept in Nonlinear Sciences* (Cambridge University Press, Cambridge, UK, 2001).

[2] A. Arenas, A. Diaz-Guilera, J. Kurths, Y. Moreno, and C. Zhou, Synchronization in complex networks, Phys. Rep. **469**, 93 (2008).

[3] S. Boccaletti, J. A. Almendral, S. Guan, I. Leyva, Z. Liu, I. Sendiña-Nadal, and Y. Zou, Explosive transitions in complex networks structure and dynamics: Percolation and synchronization, Phys. Rep. **660**, 1 (2016).

[4] Z. Wang and Z. Liu, Partial synchronization in complex networks: Chimera state, remote synchronization, and cluster synchronization, Acta Phys. Sin. **69**, 088902 (2020).

[5] D. M. Abrams and S. H. Strogatz, Chimera States for Coupled Oscillators, Phys. Rev. Lett. **93**, 174102 (2004).

[6] M. J. Panaggio and D. M. Abrams, Chimera states: Coexistence of coherence and incoherence in networks of coupled oscillators, Nonlinearity **28**, R67 (2015).

[7] Z. Wang and Z. Liu, A brief review of chimera state in empirical brain networks, Front. Physiol. **11**, 724 (2020).

[8] M. Tamaki, J. W. Bang, T. Watanabe, and Y. Sasaki, Night watch in one brain hemisphere during sleep associated with the first-night effect in humans, Curr. Biol. **26**, 1190 (2016).

[9] L. Kang, C. Tian, S. Huo, and Z. Liu, A two-layered brain network model and its chimera state, Sci. Rep. **9**, 14389 (2019).

[10] K. Bansal, J. O. Garcia, S. H. Tompson, T. Verstynen, J. M. Vettel, and S. F. Muldoon, Cognitive chimera states in human brain networks, Sci. Adv. **5**, eaau8535 (2019).

[11] S. Huo, C. Tian, M. Zheng, S. Guan, C. S. Zhou, and Z. Liu, Spatial multi-scaled chimera states of cerebral cortex network and its inherent structure-dynamics relationship in human brain, Natl. Sci. Rev. **8**, nwaa125 (2021).

[12] A. Bergner, M. Frasca, G. Sciuto, A. Buscarino, E. J. Ngamga, L. Fortuna, and J. Kurths, Remote synchronization in star networks, Phys. Rev. E **85**, 026208 (2012).

[13] L. Kang, Z. Wang, S. Huo, C. Tian, and Z. Liu, Remote synchronization in human cerebral cortex network with identical oscillators, Nonlinear Dyn. **99**, 1577 (2020).

[14] M. T. Schaub, N. O'Clery, Y. N. Billeh, J. C. Delvenne, R. Lambiotte, and M. Barahona, Graph partitions and cluster synchronization in networks of oscillators, Chaos **26**, 094821 (2016).

[15] B. Cao, Y. F. Wang, L. Wang, Y. Z. Yu, and X. G. Wang, Cluster synchronization in complex network of coupled chaotic circuits: An experimental study, Front. Phys. **13**, 130505 (2018).

[16] J. A. Acebron, S. Lozano, and A. Arenas, Amplified Signal Response in Scale-Free Networks by Collaborative Signaling, Phys. Rev. Lett. **99**, 128701 (2007).

[17] Z. Liu and T. Munakata, Scale-free topology induced double resonance in networked two-state systems, Phys. Rev. E **78**, 046111 (2008).

[18] J. Zhou, Y. Zhou, and Z. Liu, Amplification of signal response at an arbitrary node of a complex network, Phys. Rev. E **83**, 046107 (2011).

[19] C. Hens, U. Harush, S. Haber, R. Cohen, and B. Barzel, Spatiotemporal signal propagation in complex networks, Nat. Phys. **15**, 403 (2019).

[20] X. Zhang, D. Witthaut, and M. Timme, Topological Determinants of Perturbation Spreading in Networks, Phys. Rev. Lett. **125**, 218301 (2020).

[21] I. P. Ipiña, P. D. Kehoe, M. Kringelbach, H. Laufs, A. Ibañez, G. Deco, Y. S. Perl, and E. Tagliazucchi, Modeling regional changes in dynamic stability during sleep and wakefulness, NeuroImage **215**, 116833 (2020).

[22] M. I. Rabinovich, M. A. Zaks, and P. Varona, Sequential dynamics of complex networks in mind: Consciousness and creativity, Phys. Rep. **883**, 1 (2020).

[23] M. I. Rabinovich, K. J. Friston, and P. Varona, *Principles of Brain Dynamics: Global State Interactions* (MIT Press, Cambridge, MA, 2012).

[24] R. M. Hutchison and J. B. Morton, Its a matter of time: Reframing the development of cognitive control as a modification of the brain's temporal dynamics, Dev. Cogn. Neurosci. **18**, 70 (2016).

[25] S. L. Bressler and J. A. S. Kelso, Cortical coordination dynamics and cognition, Trends Cognit. Sci. **5**, 26 (2001).

[26] T. P. Meehan and S. L. Bressler, Neurocognitive networks: Findings, models, and theory, Neurosci. Biobehav. Rev. **36**, 2232 (2012).

[27] S. Majhi, B. K. Bera, D. Ghosh, and M. Perc, Chimera states in neuronal networks: A review, Phys. Life Rev. **28**, 100 (2019).

[28] R. Ma, J. Wang, and Z. Liu, Robust features of chimera states and the implementation of alternating chimera states, Europhys. Lett. **91**, 40006 (2010).

[29] Y. Zhu, Z. Zheng, and J. Yang, Chimera states on complex networks, Phys. Rev. E **89**, 022914 (2014).

[30] L. Zhang, A. E. Motter, and T. Nishikawa, Incoherence-Mediated Remote Synchronization, Phys. Rev. Lett. **118**, 174102 (2017).

[31] F. Sorrentino, L. M. Pecora, M. Hagerstrom, T. E. Murphy, and R. Roy, Complete characterization of the stability of cluster synchronization in complex dynamical networks, Sci. Adv. **2**, e1501737 (2016).

[32] Y. S. Cho, T. Nishikawa, and A. E. Motter, Stable Chimeras and Independently Synchronizable Clusters, Phys. Rev. Lett. **119**, 084101 (2017).

[33] Dynamic connetcome lab, https://www.dynamic-connectome.org/resources/.

[34] J. Hindmarsh and R. M. Rose, A model of neuronal bursting using three coupled first order differential equations, Proc. R. Soc. London, Ser. B **221**, 102 (1984).

[35] M. Dhamala, V. K. Jirsa, and M. Ding, Transitions to Synchrony in Coupled Bursting Neurons, Phys. Rev. Lett. **92**, 028101 (2004).

[36] A. Biswas, P. Kumar, D. Das, and P. Parmananda, Oscillatory activity regulation in an ensemble of autonomous mercury beating heart oscillators, Phys. Rev. E **99**, 032223 (2019).

[37] M. Chen, Y. Wang, H. Wang, W. Ren, and X. Wang, Evoking complex neuronal networks by stimulating a single neuron, Nonlinear Dyn. **88**, 2491 (2017).

[38] A. Pournaki, L. Merfort, J. Ruiz, N. E. Kouvaris, P. Hovel, and J. Hizanidis, Synchronization patterns in modular neuronal networks: A case study of *C. elegans*, Front. Appl. Math. Stat. **5**, 52 (2019).

[39] E. Montbrio and D. Pazo, Exact Mean-Field Theory Explains the Dual Role of Electrical Synapses in Collective Synchronization, Phys. Rev. Lett. **125**, 248101 (2020).

[40] T. J. Lewis and J. Rinzel, Dynamics of spiking neurons connected by both inhibitory and electrical coupling, J. Comput. Neurosci. **14**, 283 (2003).

[41] B. Pfeuty, G. Mato, D. Golomb, and D. Hansel, The combined effects of inhibitory and electrical synapses in synchrony, Neural Comput. **17**, 633 (2005).

[42] R. Phogat, S. Sinha, and P. Parmananda, Echo in complex networks, Phys. Rev. E **101**, 022216 (2020).

[43] A. Bashan, R. P. Bartsch, J. W. Kantelhardt, S. Havlin, and P. Ch. Ivanov, Network physiology reveals relations between network topology and physiologic function, Nat. Commun. **3**, 702 (2012).